# Multiple Critical Couplings and Sensing in a Microresonator-Waveguide System

Nirmalendu Acharyya and Gregory Kozyreff
*Optique Nonlinéaire Théorique, Université libre de Bruxelles (ULB), CP 231, Campus de la Plaine, 1050 Bruxelles, Belgium*
(Received 3 July 2017; revised manuscript received 21 August 2017; published 27 September 2017)

We study the optical transmission of a waveguide that is side coupled to a high-$Q$ circular microresonator. The coupling is critical if the intrinsic resonator losses equal the coupling losses to the waveguide. When this happens, the transmittance of the waveguide displays resonance dips with maximal depth as the frequency is swept through the resonators' resonances. We show that multiple configurations, parametrized by the minimal distance between the resonator and the waveguide, can lead to critical coupling. Indeed, for a sufficiently large resonator radius, the flow of power between the waveguide and the resonator can change sign several times within a single pass. This leads to an oscillatory coupling parameter as a function of the separation distance. As a result, multiple geometrical configurations can lead to critical coupling, even if the waveguide lies in the equatorial plane of the resonator. These results are explained using coupled-mode theory and full-wave numerical simulations. In the vicinity of secondary or higher-order critical coupling, the depth of the transmittance dip is very sensitive to the environment. We discuss how this effect can be exploited for sensing purpose. Alternatively, by actively controlling the environment in the secondary critical configuration, the waveguide-resonator system can be driven as an optical switch.

DOI: 10.1103/PhysRevApplied.8.034029

## I. INTRODUCTION

Circular resonators such as microspheres, microtoroids, wedge resonators, and microrings have dramatically improved the quality of light-matter interaction in cavities, in the sense of enhanced interaction strength and spectral purity of the recorded signals. With losses only limited by intrinsic material absorption, quality factors $Q$ reaching $3 \times 10^{11}$ have been demonstrated [1]. The detection of small wavelength shifts of the resonances of these cavities is the basis of very sensitive detectors [2–6]. Nonlinear effects are also enhanced, with a reduced threshold for parametric oscillations [7–9] and second-harmonic generation [10], and with a strong current focus on frequency comb generation [11,12]. In this respect, at the photon level, phase matching corresponds to angular momentum conservation and follows the associated composition rules of quantum mechanics [13]. Thanks to the high $Q$, surface-second-harmonic generation mediated by as few as one hundred *small* molecules (equivalent in mass to a single protein) has been demonstrated [14]. Furthermore, the large $Q$-to-$V$ ratios, where $V$ is the mode volume, makes these cavities particularly useful to study quantum electrodynamics [15] and quantum optics [16]. Currently, the field is steadily progressing towards integrated application, with high-$Q$ microresonators being demonstrated with silicon [17,18] and silicon-nitride platforms [19–22].

The most effective way to pump and interrogate the resonances of these resonators is to couple them with a waveguide. A detailed theory of this coupling has been worked out and demonstrated experimentally before [23–25], with special emphasis on critical coupling, where ideally all the optical power injected in the waveguide can be dissipated by the resonator. The external waveguide, through its coupling to the resonator, also represents an adjustable loss mechanism and can therefore be a key parameter in the hands of an experimentalist, notably to control the threshold of optical parametric oscillations and quantum light production [26].

Recently, it has been pointed out that multiple critical configurations can exist if the waveguide is buried under the microresonator [27,28]. As the vertical gap between the waveguide is decreased, a pair of critical-coupling configurations are demonstrated, in addition to the usual one. Moreover, within the narrow range of gaps between the two newly found critical-coupling distances, the system reverts to an undercoupling state. Until now, it was assumed that such an exotic situation was only possible if the waveguide lies in a different plane from that of the resonator [27,28]. However, this is not the case. We show that similar multiple critical couplings can be found with microresonators *side coupled* to a waveguide. Moreover, our analysis shows that an arbitrary number of critical-coupling configurations can be achieved, depending on the microresonator radius, see Fig. 1. We demonstrate this possibility using coupled-mode theory and finite-element numerical simulations, which are in full quantitative agreement.

As can be seen in Fig. 1, the transmission at resonance, $T(\omega_R)$, exhibits very sharp features in the multicritical regime when plotted as a function of the waveguide-resonator distance. In this paper, we will show how this

 

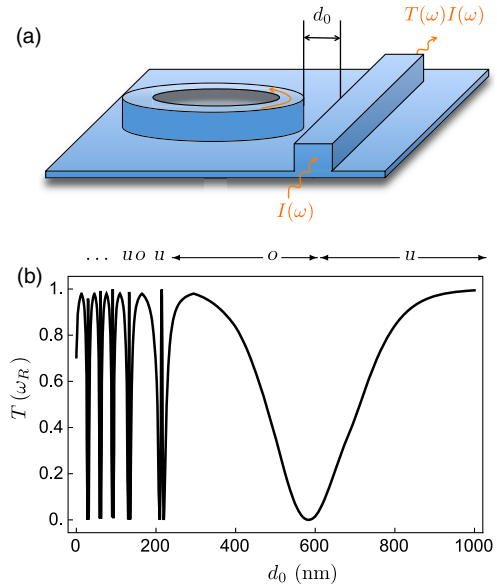


FIG. 1. (a) Schematic of the waveguide-resonator system. (b) Transmittance at resonance ($\omega = \omega_R$) as a function of coupling distance $d_0$ for a 100-$\mu$m-radius silicon (refractive index = 3.48) ring coupled to a ridge waveguide on a $SiO_2$ substrate (refractive index = 1.45). Microring and waveguide width, $w = 200$ nm. Height, 400 nm. Base height, 50 nm. $Q = 4.4 \times 10^5$, $\lambda \approx 1.55$ $\mu$m, $|\tilde{\alpha}| = 0.99$. The near-zero transmittance at $d_0 \approx 600$ nm is the usual critical-coupling situation. Additional critical-coupling distances are found for $d_0 < 210$ nm, always appearing in pairs. The letters "$u$" and "$o$" indicate undercoupled and overcoupled regions, respectively.

can be exploited for sensing purposes. Indeed, the transmission increases very rapidly as soon as one departs from the conditions of critical coupling. Rather than detecting the shift of spectral resonance as a response to environmental change, we propose to detect the increase of transmission, or changes in extinction ratios.

In what follows, we first briefly review the general derivation of the intensity transmittance of the waveguide-microresonator system. This will be necessary to explain and derive simple analytical estimates of the emergence of multiple critical couplings. Next, we discuss the exploitation of this effect for sensing or switching purposes. Finally, we conclude.

## II. THEORY OF MULTIPLE CRITICAL COUPLINGS

We focus here on ideal coupling, whereby the waveguide is a single mode and parasitic losses are negligible [23,24,29,30]. The direct interaction between the waveguide and the resonator usually takes place in a narrow region of space, where the resonator can be regarded as a segment of curved waveguide as in Ref. [31]. Let us assume for simplicity that the two waveguides have identical width $w$, propagation constant $\bar{\beta}$ at infinite separation, and that

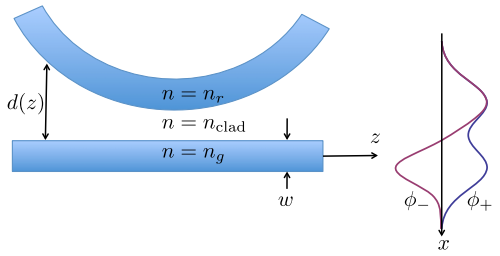


FIG. 2. Schematic of the coupling region and the local profiles of the propagation eigenmodes $\phi_\pm$, between a waveguide and microresonator. $n_g$, guiding refractive index; $n_{\text{clad}}$, cladding refractive index; $n_r$, resonator refracting index. Throughout this paper, we will assume that $n_r = n_g$.

they have the same refractive index, see Fig. 2. Departures from this symmetrical situation can easily be taken into account in principle (an accurate asymptotic formula of the dispersion relation for curved waveguide is given in Ref. [32]). If the local distance $d(z)$ varies slowly compared to the wavelength, then the Helmholtz equation can be treated by perturbation [33]. In this frame, the field is expanded in terms of the local modes of propagation as

$$\psi \approx a_+(z)\phi_+(x,y,z) + a_-(z)\phi_-(x,y,z). \tag{1}$$

Above, $\phi_+(x,y,z)$ and $\phi_-(x,y,z)$ are, respectively, symmetric and antisymmetric with respect to the middle point and are normalized such that

$$\langle \phi_i | \phi_j \rangle = \iint \phi_i^*(x,y,z)\phi_j(x,y,z)dxdy = \delta_{i,j}, \quad i,j = \pm. \tag{2}$$

The evolution of $a_+(z)$ and $a_-(z)$ is given by [33]

$$\frac{da_\pm}{dz} \approx i\beta_\pm(z)a_\pm, \tag{3}$$

where $\beta_\pm(z)$ are the local propagation constants. The calculation of the local modes and their propagation constants is a 2D problem for each value of $z$. It can be solved by standard softwares such as LUMERICAL, COMSOL, or the spectral index method [34]. Note that the graph of $\beta_\pm(z)$ allows one to objectively determine the extent of the coupling region: outside it, the local propagation constants are indistinguishable from their asymptotic values, see Fig. 3.

Given the amplitudes $a_\pm(z)$ associated with the symmetric and antisymmetric modes, the amplitudes in the waveguide and in the resonator can be retrieved as

$$a_g(z) = (a_- + a_+)/\sqrt{2}, \quad a_r(z) = (a_- - a_+)/\sqrt{2}. \tag{4}$$

Combining the above relations, it is straightforward to derive the following matrix relation between the amplitudes at the entrance ($z = -z_c/2$) and exit ($z = z_c/2$) of the coupling zone:

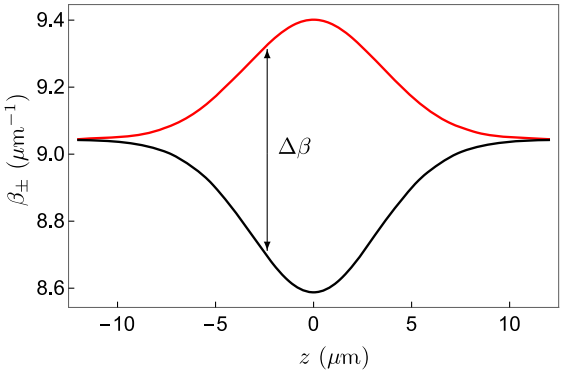


FIG. 3. Propagation constants $\beta_\pm(z)$ for the symmetric and antisymmetric modes of propagation in the straight and curved waveguide systems. $n_g = 3.48$; $n_{\text{clad}} = 1.45$; resonator radius $R = 100$ $\mu$m; $\lambda = 1.55$ $\mu$m; width of both waveguides, $w = 200$ nm. Minimal separation $d_0 = 200$ nm.

$$\begin{pmatrix} a_{g,2} \\ a_{r,2} \end{pmatrix} = M \begin{pmatrix} a_{g,1} \\ a_{r,1} \end{pmatrix}. \tag{5}$$

The matrix $M$ is given by

$$M = \frac{1}{2}\begin{pmatrix} 1 & 1 \\ 1 & -1 \end{pmatrix}\begin{pmatrix} e^{i\int_{-z_c/2}^{z_c/2}\beta_+ dz} & 0 \\ 0 & e^{i\int_{-z_c/2}^{z_c/2}\beta_- dz} \end{pmatrix}\begin{pmatrix} 1 & 1 \\ 1 & -1 \end{pmatrix}. \tag{6}$$

Above, $z_c$ can be any sufficiently large value that $|\Delta\beta(z_c)| \ll 1$. If we write

$$\beta_\pm(z) = \bar{\beta} \pm \Delta\beta(z)/2 \tag{7}$$

and introduce

$$\delta = \frac{1}{2}\int_{-z_c/2}^{z_c/2} \Delta\beta(z)dz, \tag{8}$$

then $M$ assumes the familiar form

$$M = e^{i\bar{\beta}z_c}\begin{pmatrix} \cos\delta & i\sin\delta \\ i\sin\delta & \cos\delta \end{pmatrix}. \tag{9}$$

Following Yariv [25], Eq. (5) is completed by the feedback condition

$$a_{r,1} = \tilde{\alpha} a_{r,2}, \tag{10}$$

where the complex constant $\tilde{\alpha}$ accounts for propagation in the resonator outside the coupling region. Thus, one easily obtains the intensity transmission coefficient of the waveguide-resonator system

$$a_{g,2}/a_{g,1} = e^{i\bar{\beta}z_c}\frac{\cos\delta - \tilde{\alpha}e^{i\bar{\beta}z_c}}{1 - \tilde{\alpha}e^{i\bar{\beta}z_c}\cos\delta}, \tag{11}$$

$$\rightarrow T = \left|\frac{\cos\delta - \tilde{\alpha}e^{i\bar{\beta}z_c}}{1 - \tilde{\alpha}e^{i\bar{\beta}z_c}\cos\delta}\right|^2. \tag{12}$$

To make contact with notations in previous works [24,25], we write

$$\cos\delta = |t|e^{i\xi}, \quad \sin\delta = \kappa, \quad \text{and} \quad \tilde{\alpha}e^{i\bar{\beta}z_c} = |\tilde{\alpha}|e^{i\varphi}, \tag{13}$$

where $\xi = 0$ or $\pi$, according to the sign of $\cos\delta$. Above, $t$ is the single-pass transmission coefficient and $\varphi \pm \xi$ is the phase accumulated by a traveling wave in the microresonator over a complete round-trip, whether it is given by $\phi_-(x)$ or $\phi_+(x)$ in the coupling region. $\varphi$ is a function of the injection frequency $\omega$ through the dispersion relation within the resonator. Resonant injection $\omega = \omega_R$ happens if

$$\varphi + \xi = 2\ell\pi, \qquad \ell \in \mathbb{N}. \tag{14}$$

The transmission at resonance is then

$$T(\omega_R) = \left(\frac{|\cos\delta| - |\tilde{\alpha}|}{1 - |\tilde{\alpha}\cos\delta|}\right)^2. \tag{15}$$

Hence, the condition for critical coupling, $T(\omega_R) = 0$, is given by the well-known formula [25]

$$|t| = |\tilde{\alpha}|. \tag{16}$$

Typical microcavities have a very large $Q$ factor, so that $|\tilde{\alpha}| = \exp(-n_g k\pi R/Q) \approx 1$. Consequently, critical coupling requires $|\cos\delta| \approx 1$ and, in usual situations, this is achieved for a very small single-pass phase shift: $\delta \ll 1$. However, it is easy to see in Eq. (15) that $T(\omega_R)$ is a $\pi$-periodic function of $\delta$. If the single-pass interaction is sufficiently strong that $\delta > \pi$, then multiple critical couplings arise.

With very good accuracy, $\Delta\beta$ decreases exponentially with $d$, at least for large enough $d$:

$$\Delta\beta(z) \approx \Delta\beta_0 e^{-md(z)}, \tag{17}$$

where $\Delta\beta_0$ is the splitting of propagation constants at contact. In the simplified situation where the waveguide and ring have infinite height, the decaying constant $m$ is simply given by

$$m = \sqrt{\bar{\beta}^2 - n_{\text{clad}}^2 k^2}, \tag{18}$$

and this expression remains applicable with reasonable accuracy even for realistic situations such as in Fig. 1. Given (17), with $d \approx d_0 + z^2/(2R)$, one immediately obtains

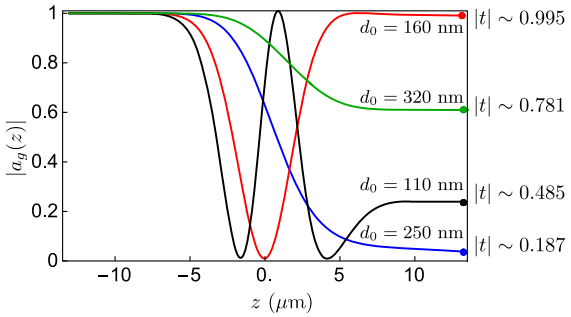


FIG. 4. Waveguide field amplitude in the single-pass configuration for various values of $d_0$. The single-pass transmission coefficient is given by $|t| = |\cos\delta| = \lim_{z\to\infty}|a_g(z)|$. $n_g = 3.48$, $n_{\text{clad}} = 1.45$, $R = 100$ $\mu$m, $\lambda = 1.55$ $\mu$m, $w = 200$ nm, infinite height. As $d_0$ is decreased, $|t|$ varies nonmonotonically, allowing the critical condition $|t| = |\tilde{\alpha}| \leftrightarrow T(\omega_R) \approx 0$ to be achieved for several values of $d_0$, see Fig. 1(b).

$$\delta \approx \frac{1}{2}\int_{-\infty}^{\infty} \Delta\beta(z)dz = \Delta\beta_0 e^{-md_0}\sqrt{\frac{\pi R}{2m}}. \tag{19}$$

In this expression, $\exp(md_0)/\Delta\beta_0$ can be viewed as the effective coherence length of interaction between the waveguide and the portion of resonator with which it interacts. On the other hand, $\sqrt{\pi R/2m}$ is the effective coupling length [35]. Multiple critical couplings require the effective coupling length to exceed the effective coherence length.

This situation is depicted in Fig. 4. There, the field amplitude is computed in the single-pass configuration, i.e., without the feedback provided by the cavity for various values of $d_0$. For simplicity of calculation, we assumed in that figure an infinite height, both for the waveguide and the microresonator. For sufficiently small $d_0$ the coupling length exceeds the coherence length, so that optical energy is transferred back and forth several times between the waveguide and the ring. Furthermore, Fig. 5 shows a finite-element simulation (COMSOL MUTLIPHYSICS 5.3) of a ring

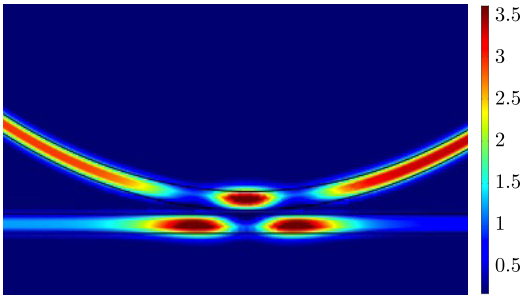


FIG. 5. Field-intensity distribution in a waveguide resonantly coupled to a ring resonator at a high-order critical-coupling distance. The higher-order character of the coupling is attested to by the presence of "hot spots" in the waveguide. $R = 30$ $\mu$m, $d_0 = 46$ nm, $w = 200$ nm, and infinite height assumed.

and waveguide at "third-order" critical coupling, in the sense that $\delta \approx (3-1)\pi$, or equivalently, that the effective coupling length is twice the effective coherence length. Note the presence of three "hot spots"; these result from interferences within the coupling region, combined with intensity buildup in the cavity.

From what precedes, the minimal radius for multiple critical couplings is the one for which $\delta = \pi$ as $d_0 \to 0$, i.e., at contact coupling,

$$\Delta\beta_0\sqrt{\frac{\pi R_{\text{min}}}{2m}} = \pi. \tag{20}$$

Above, to evaluate $\Delta\beta_0$, we note that as $d_0 \to 0$, the resonator plus the waveguide locally make a single waveguide of width $2w$. Then, $\Delta\beta_0$ is the separation between the fundamental even and odd modes (e.g., $\text{TE}_0$ vs $\text{TE}_1$) of that waveguide. A precise estimation requires one to solve the transcendental equation for the propagation constants of the waveguide. As a general rule,

$$\Delta\beta_0 \approx \frac{g}{w}, \tag{21}$$

for some constant $g$ that depends on the refractive index and geometry of the waveguide. Substituting in Eq. (20), we finally obtain

$$R_{\text{min}} = \left(\frac{2\pi m\lambda}{g^2}\right)\frac{w^2}{\lambda} \equiv \frac{4\pi^2\sqrt{n_{\text{eff}}^2 - n_{\text{clad}}^2}}{g^2}\frac{w^2}{\lambda}, \tag{22}$$

where the left factor is dimensionless, $m$ is defined in Eq. (18), and the effective refractive index is defined as $n_{\text{eff}} = \bar{\beta}/k$. The increase of $R_{\text{min}}$ in $w$ is consistent with intuition, since a larger value of $w$ leads to a smaller evanescent field outside the waveguide, hence a weaker coupling and a longer coherence length.

The graph of $R_{\text{min}}$ is computed numerically for waveguides of infinite height in Fig. 6, confirming the trend given in Eq. (22). The values of $\Delta\beta_0$ and $m$ are evaluated by solving the transcendental equation for a slab waveguide of width $2w$ and substituted in Eq. (20) to obtain $R_{\text{min}}$. Alternatively, we ran COMSOL simulations to compute the single-pass transmittance $t$ of a straight slab waveguide in contact with a curved slab waveguide. We increased the radius of curvature until obtaining $t = -1$ (i.e., $\delta = \pi$) and found very good agreement with the analytical results.

If we consider ridge waveguides, the transmission curve shown in Fig. 1(b) can accurately be reproduced by substituting Eq. (19) into Eq. (15) with appropriately chosen values of $\Delta\beta_0$ and $m$. For the specific parameters of Fig. 1, fitting values are $\Delta\beta_0 = 4.47$ $\mu\text{m}^{-1}$ and $m = 8.42$ $\mu\text{m}^{-1}$.

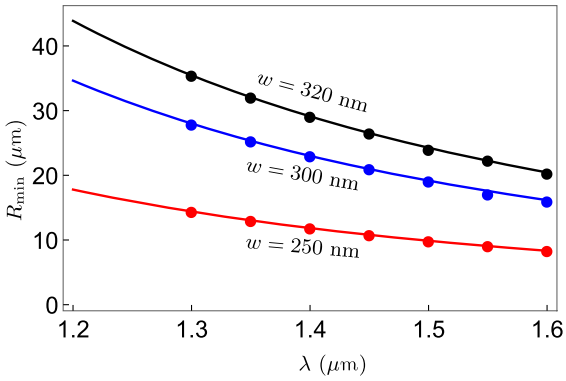


FIG. 6. Minimal ring radius leading to multiple critical couplings as a function of wavelength for various waveguide widths. Infinite height assumed. $n_g = 3.48$, $n_{\text{clad}} = 1.45$. Full line, analytical results. Dots, COMSOL simulation.

## III. SENSING AND SWITCHING APPLICATIONS

Once the conditions for the configurations of multiple critical couplings are established, we note that the sharp features in the dependence of $T$ on $d_0$ (see Fig. 1 and inset of Fig. 7) could serve as the basis of a detection principle. Indeed, a change in the cladding refractive index $n_{\text{clad}}$, or in the guiding index $n_g$ would amount to effectively changing $d_0$.

Rather than monitoring the spectral shift of resonances in the transmission spectrum, we propose to monitor changes in the transmission dip at resonance. This is slightly different from the previous intensity-detection scheme, such as Ref. [36], where one monitors the transmitted intensity at a fixed, near-resonant, wavelength, as the cladding index is varied. In that case, variations of transmitted intensity are due to resonance shift. Here, we propose to follow the resonance peak and monitor the depth of the resonant transmission dip as the refractive index is changed.

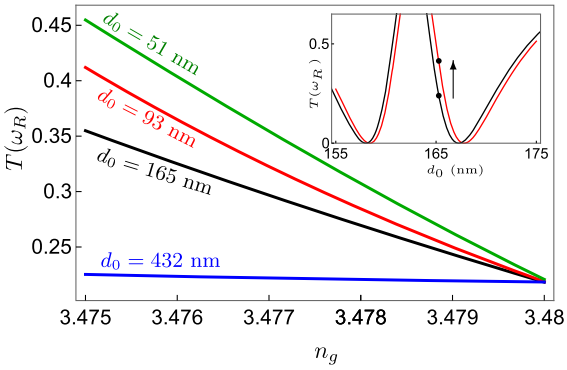


FIG. 7. Resonant transmission as a function of $n_g$ for values of $d_0$ near critical values. Inset: transmission curve in the vicinity of $d_0 = 165$ nm, $w = 200$ nm, $R = 100\,\mu$m, $n_{\text{clas}} = 1.45$, $\lambda \approx 1.55$ nm, and $n_g = 3.48$ (black) or $n_g = 3.475$ (red curve).

Let the incident power be centered on the resonance and given by $I(\omega_R)$. A change of the guiding index

$$n_g \to n_g + \Delta n_g \tag{23}$$

leads to a transmission change

$$T(\omega_R) \to T(\omega_R) + \frac{\partial T(\omega_R)}{\partial n_g}\Delta n_g, \tag{24}$$

and, hence, to change in transmitted power

$$I(\omega_R)\frac{\partial T(\omega_R)}{\partial n_g}\Delta n_g. \tag{25}$$

Given the noise equivalent power (NEP) of the photodetector and the measurement bandwidth $\Delta f$, the smallest detectable index change is given by [37]

$$\Delta n_{g,\min} = \frac{\text{NEP}\sqrt{\Delta f}}{I(\omega_R)\left|\frac{\partial T(\omega_R)}{\partial n_g}\right|}. \tag{26}$$

While the value of $|\partial T/\partial n_g|$ is rather modest around the first critical distance, it raises sharply in the vicinity of higher-order critical-coupling distances, see Fig. 7. Note from the inset of Fig. 7 that the slope $|\partial T/\partial d_0|$ is highest on the undercoupling side of the critical point.

Assuming an NEP on the order of 10 pW/$\sqrt{\text{Hz}}$ [37], an input source power of $I(\omega_R) = 10$ mW with a frequency bandwidth of 1 GHz, Table I gives limits of detection (LOD) $\Delta n_{g,\min}$ in the vicinity of various critical-coupling distances. With the numbers assumed here ($\lambda \approx 1.55\,\mu$m, cavity radius $R = 100\,\mu$m, $n_g = 3.48$, waveguide width $w = 200$ nm) one finds an LOD of $7.5 \times 10^{-7}$ refractive index unit (RIU). This should not be regarded as an ultimate value, as better sources can in principle be used, with higher incident power and narrower bandwidth. Also, we see from Table I that the LOD improves substantially with the order of critical coupling. Higher-order critical coupling, corresponding to smaller $d_0$ is liable to yield even smaller LOD. However, the rapidity of oscillation becomes such that numerical investigations become challenging in that region of parameters.

TABLE I. Limit of detection through intensity measurements in the vicinity of critical points. Same resonator and waveguide parameters as in Fig. 4. NEP = 10 pW/$\sqrt{\text{Hz}}$. Detection bandwidth $\Delta f = 1$ GHz. Input power $I(\omega_R) = 10$ mW.

| Critical region | $d_0$ (nm) | $\lvert\partial T/\partial n_g\rvert$ | $\Delta n_{g,\min}$ |
|---|---|---|---|
| 1 | 432 | 1 | $3.2 \times 10^{-5}$ |
| 2 | 165 | 25 | $1.3 \times 10^{-6}$ |
| 3 | 93 | 31 | $1.0 \times 10^{-6}$ |
| 4 | 51 | 42 | $7.5 \times 10^{-7}$ |

Alternatively to the above application, one may envisage actively inducing a change of refractive index in order to induce a desired change $\Delta I_{\text{out}}(\omega_R)$ in the output intensity. In this switching setup, the required change is, simply

$$\Delta n_g = \frac{\Delta I_{\text{out}}(\omega_R)}{I(\omega_R)\left|\frac{\partial T(\omega_R)}{\partial n_g}\right|}. \tag{27}$$

It is a simple matter to show that $|\partial T/\partial d_0|$ or $|\partial T/\partial n_g|$ scales as $\sqrt{Q}$: In the region of higher-order coupling, critical-coupling configurations come in pairs, flanking a state of complete transmission $T(\omega_R) = 1$, see Fig. 1. Let us assume that, for the appropriate value of $d_0$, the value $n_g^*$ of the guiding refractive index makes $|t| = 1$, and, hence, $T = 1$. In the vicinity of this value, we have

$$|t| \sim 1 - |t''(n_g^*)|\frac{(n_g - n_g^*)^2}{2}. \tag{28}$$

On the other hand,

$$|\tilde{\alpha}| \sim 1 - \epsilon, \quad \text{with} \quad \epsilon \propto 1/Q \ll 1. \tag{29}$$

The nearest critical-coupling configuration, $|t| = |\tilde{\alpha}|$, thus happens for

$$|n_g - n_g^*| \sim \sqrt{2\epsilon/|t''(n_g^*)|}. \tag{30}$$

Since the resonant transmittance changes from 1 to 0 over this change of refractive index, the average slope of this dependence is proportional to $1/\sqrt{\epsilon}$, i.e., to $\sqrt{Q}$.

## IV. CONCLUSIONS

In this work, we have expanded the classical theory of waveguide-resonator coupling and shown that, contrary to common assumption, distances for multiple critical couplings *can* exist when the bus waveguide lies in the same plane as the resonator. This effect exists as soon as the resonator radius exceeds a critical radius, for which we give an analytical estimate as a function of wavelength and waveguide transverse dimension. The present treatment, being expressed in terms of the local splitting of propagation constants $\Delta\beta(z)$, can directly be transposed to other geometries, e.g., racetrack resonators or waveguide and ring lying in different planes. In the case of a circular resonator side coupled to a waveguide, the function $\Delta\beta(z)$ has a Gaussian profile with width controlled by the cavity radius. Thus, the effective coupling length was found to be $\sqrt{\pi R/2m}$. For racetrack resonators, the splitting function $\Delta\beta(z)$ exhibits a plateau around $z = 0$. In all cases, the space dependence of $\Delta\beta(z)$ makes the single-pass coupling problem distinct from that of coupled straight parallel waveguides.

As we have shown, multiple critical couplings can be exploited as an alternative detection principle. Equally, the on or off switching of resonances in the transmission spectrum could be used as an optical gate. More generally, this study shows that the single-pass transmission parameter $t$, and hence the coupling parameter $\kappa = \sqrt{1 - t^2}$, may vary in a much more complicated way than anticipated as a function of the waveguide-resonator distance $d_0$. This behavior may become important to consider in future designs of photonic integrated circuits in which microresonators are expected to play major roles. Although we have illustrated it with silicon refractive index and telecom wavelength, the theory presented here is general and independent of the material considered. Let us note that water strongly absorbs light at $\lambda = 1.55$ $\mu$m, so that sensing in an aqueous environment is more suitably done at $\lambda = 1$ $\mu$m. We have therefore checked that all our conclusions hold with $Al_2O_3$ waveguides with realistic fabrication parameters operating around 1 $\mu$m.

## ACKNOWLEDGMENTS

This project has received funding from the European Union's Horizon 2020 research and innovation programme under Grant No. 634928. G. K. is a research associate with the Fund for Scientific Research-FNRS. We thank Pascal Kockaert for useful discussions, as well as Johann Toudert, Johann Osmond, Michiel de Goedde, and Sonia García Blanco for communicating precious details on device fabrication.

[1] Anatoliy A. Savchenkov, Andrey B. Matsko, Vladimir S. Ilchenko, and Lute Maleki, Optical resonators with ten million finesse, Opt. Express **15**, 6768 (2007).
[2] S. Arnold, M. Khoshsima, I. Teraoka, S. Holler, and F. Vollmer, Shift of whispering-gallery modes in microspheres by protein adsorption, Opt. Lett. **28**, 272 (2003).
[3] F. Vollmer, S. Arnold, and D. Keng, Single virus detection from the reactive shift of a whispering-gallery mode, Proc. Natl. Acad. Sci. U.S.A. **105**, 20701 (2008).
[4] Lina He, Şahin Kaya Özdemir, Jiangang Zhu, Woosung Kim, and Lan Yang, Detecting single viruses and nanoparticles using whispering gallery microlasers, Nat. Nanotechnol. **6**, 428 (2011).
[5] F. Vollmer and L. Yan, Label-free detection with high-$Q$ microcavities: A review of biosensing mechanisms for integrated devices, Nanophotonics **1**, 267 (2012).
[6] Matthew Frenkel and Zhixiong Guo, On-chip, dynamic, and cryogenic temperature monitoring via PDMS micro-bead coatings, J. Polym. Sci., Part B: Polym. Phys. **54**, 1118 (2016).
[7] T. J. Kippenberg, S. M. Spillane, and K. J. Vahala, Kerr-Nonlinearity Optical Parametric Oscillation in an Ultrahigh-$Q$ Toroid Microcavity, Phys. Rev. Lett. **93**, 083904 (2004).
[8] A. A. Savchenkov, A. B. Matsko, D. Strekalov, M. Mohageg, V. S. Ilchenko, and L. Maleki, Low Threshold

Optical Oscillations in a Whispering Gallery Mode $CaF_2$ Resonator, Phys. Rev. Lett. **93**, 243905 (2004).

[9] J. U. Fürst, D. V. Strekalov, D. Elser, A. Aiello, U. L. Andersen, Ch. Marquardt, and G. Leuchs, Low-Threshold Optical Parametric Oscillations in a Whispering Gallery Mode Resonator, Phys. Rev. Lett. **105**, 263904 (2010).

[10] V. S. Ilchenko, A. A. Savchenkov, A. B. Matsko, and L. Maleki, Nonlinear Optics and Crystalline Whispering Gallery Mode Cavities, Phys. Rev. Lett. **92**, 043903 (2004).

[11] Yanne K. Chembo and Nan Yu, Modal expansion approach to optical-frequency-comb generation with monolithic whispering-gallery-mode resonators, Phys. Rev. A **82**, 033801 (2010).

[12] Yoshitomo Okawachi, Kasturi Saha, Jacob S. Levy, Y. Henry Wen, Michal Lipson, and Alexander L. Gaeta, Octave-spanning frequency comb generation in a silicon nitride chip, Opt. Lett. **36**, 3398 (2011).

[13] G. Kozyreff, J. L. Dominguez Juarez, and Jordi Martorell, Whispering-gallery-mode phase matching for surface second-order nonlinear optical processes in spherical microresonators, Phys. Rev. A **77**, 043817 (2008).

[14] J. L. Dominguez-Juarez, G. Kozyreff, and J. Martorell, Whispering gallery microresonators for second harmonic light generation from a low number of small molecules, Nat. Commun. **2**, 254 (2011).

[15] Takao Aoki, Barak Dayan, Elizabeth Wilcut, Warwick P. Bowen, A. Scott Parkins, T. J. Kippenberg, K. J Vahala, and H. J. Kimble, Observation of strong coupling between one atom and a monolithic microresonator, Nature (London) **443**, 671 (2006).

[16] Dmitry V. Strekalov, Christoph Marquardt, Andrey B. Matsko, Harald G. L. Schwefel, and Gerd Leuchs, Nonlinear and quantum optics with whispering gallery resonators, J. Opt. **18**, 123002 (2016).

[17] W. Bogaerts, P. De Heyn, T. Van Vaerenbergh, K. De Vos, S. Kumar Selvaraja, T. Claes, P. Dumon, P. Bienstman, D. Van Thourhout, and R. Baets, Silicon microring resonators, Laser Photonics Rev. **6**, 47 (2012).

[18] Mohammad Soltani, V. Ilchenko, A. Matsko, A. Savchenkov, J. Schlafer, C. Ryan, and L. Maleki, Ultrahigh $Q$ whispering gallery mode electro-optic resonators on a silicon photonic chip, Opt. Lett. **41**, 4375 (2016).

[19] Ming-Chun Tien, Jared F. Bauters, Martijn J. R. Heck, Daryl T. Spencer, Daniel J. Blumenthal, and John E. Bowers, Ultra-high quality factor planar $Si_3N_4$ ring resonators on Si substrates, Opt. Express **19**, 13551 (2011).

[20] Daryl T. Spencer, Jared F. Bauters, Martijn J. R. Heck, and John E. Bowers, Integrated waveguide coupled $Si_3N_4$ resonators in the ultrahigh-$Q$ regime, Optica **1**, 153 (2014).

[21] Yi Xuan, Yang Liu, Leo T. Varghese, Andrew J. Metcalf, Xiaoxiao Xue, Pei-Hsun Wang, Kyunghun Han, Jose A. Jaramillo-Villegas, Abdullah Al Noman, Cong Wang, Sangsik Kim, Min Teng, Yun Jo Lee, Ben Niu, Li Fan, Jian Wang, Daniel E. Leaird, Andrew M. Weiner, and Minghao Qi, High-$Q$ silicon nitride microresonators exhibiting low-power frequency comb initiation, Optica **3**, 1171 (2016).

[22] Xingchen Ji, Felippe A. S. Barbosa, Samantha P. Roberts, Avik Dutt, Jaime Cardenas, Yoshitomo Okawachi, Alex Bryant, Alexander L. Gaeta, and Michal Lipson, Ultra-low-loss on-chip resonators with sub-milliwatt parametric oscillation threshold, Optica **4**, 619 (2017).

[23] M. L. Gorodetsky and V. S. Ilchenko, Optical microsphere resonators: Optimal coupling to high-$Q$ whispering-gallery modes, J. Opt. Soc. Am. B **16**, 147 (1999).

[24] M. Cai, O. Painter, and K. J. Vahala, Observation of Critical Coupling in a Fiber Taper to Silica-Microsphere Whispering-Gallery Mode System, Phys. Rev. Lett. **85**, 74 (2000).

[25] Amnon Yariv, Universal relations for coupling of optical power between microresonators and dielectric waveguides, Electron. Lett. **36**, 321 (2000).

[26] J. U. Fürst, D. V. Strekalov, D. Elser, A. Aiello, U. L. Andersen, Ch. Marquardt, and G. Leuchs, Quantum Light from a Whispering-Gallery-Mode Disk Resonator, Phys. Rev. Lett. **106**, 113901 (2011).

[27] M. Ghulinyan, F. Ramiro-Manzano, N. Prtljaga, R. Guider, I. Carusotto, A. Pitanti, G. Pucker, and L. Pavesi, Oscillatory Vertical Coupling between a Whispering-Gallery Resonator and a Bus Waveguide, Phys. Rev. Lett. **110**, 163901 (2013).

[28] Fabio Turri, Fernando Ramiro-Manzano, Iacopo Carusotto, Mher Ghulinyan, Georg Pucker, and Lorenzo Pavesi, Wavelength dependence of a vertically coupled resonator-waveguide system, J. Lightwave Technol. **34**, 5385 (2016).

[29] S. M. Spillane, T. J. Kippenberg, O. J. Painter, and K. J. Vahala, Ideality in a Fiber-Taper-Coupled Microresonator System for Application to Cavity Quantum Electrodynamics, Phys. Rev. Lett. **91**, 043902 (2003).

[30] Martin H. P. Pfeiffer, Junqiu Liu, Michael Geiselmann, and Tobias J. Kippenberg, Coupling Ideality of Integrated Planar High-$Q$ Microresonators, Phys. Rev. Applied **7**, 024026 (2017).

[31] D. R. Rowland and J. D. Love, Evanescent wave coupling of whispering gallery modes of a dielectric cylinder, IEE Proc. J **140**, 177 (1993).

[32] G. Kozyreff and N. Acharyya, Dispersion relations and bending losses of cylindrical and spherical shells, slabs, and slot waveguides, Opt. Express **24**, 28204 (2016).

[33] Allan W. Snyder and John D. Love, *Optical Waveguide Theory* (Chapman and Hall, New York, 1983).

[34] S. V. Burke, The spectral index method for semiconductor rib and ridge waveguides, Prog. Electromagn. Res. **10**, 41 (1995).

[35] Yann G. Boucher, Analytical model for the coupling constant of a directional coupler in terms of slab waveguides, Opt. Eng. (Bellingham, Wash.) **53**, 071810 (2014).

[36] Chung-Yen Chao, W. Fung, and L. J. Guo, Polymer microring resonators for biochemical sensing applications, IEEE J. Sel. Top. Quantum Electron. **12**, 134 (2006).

[37] Verena Mackowiak, Jens Peupelmann, Yi Ma, and Anthony Gorges, NEP–Noise Equivalent Power, White Paper, Thorlabs (2015).